Convection in the presence of a first-order phase change

Shinichi Sakurai,[1,2] Armin Tschammer,[3] Werner Pesch,[3] and Guenter Ahlers[1]
[1]*Department of Physics and Center for Nonlinear Science, University of California at Santa Barbara, Santa Barbara, California 93106*
[2]*Department of Polymer Science and Engineering, Kyoto Institute of Technology, Matsugasaki, Sakyo-ku, Kyoto 606-8585, Japan*
[3]*Physikalisches Institut der Universität Bayreuth, 95440 Bayreuth, Germany*
(Received 19 January 1999)

We report experimental and theoretical results for two-phase convection in a thin horizontal layer of a fluid with a first-order phase change and heated from below. A top layer of the nematic phase of a liquid crystal is located above the bottom layer of the isotropic phase of the same substance. A horizontal field of 1000 G is applied in order to align the director of the nematic phase. Over some ranges of the thickness of the isotropic phase, and in sufficiently large thermal gradients, the more dense nematic phase can be stably stratified above the less dense isotropic one, with a stable interface between them. Based on the equations of motion derived for this problem by Busse and Schubert [J. Fluid Mech. **46**, 801 (1971)], we evaluate the bifurcation lines between the quiescent and convecting states and the corresponding critical wave vectors as a function of the interface position. We report experimental measurements based on Nusselt-number determinations for the locations of the bifurcation lines. They are in good agreement with the theoretical results. We also report approximate determinations of the critical wave numbers which are semiquantitatively consistent with the theory. A great diversity of patterns is observed in the convecting states, including normal and parallel rolls, rolls with defects and disorder, target patterns and spirals, and cellular flow with upflow or downflow at the cell center. These patterns are discussed in terms of the breaking of the mirror symmetry at the horizontal midplane by the interface, and in terms of the orienting effects of the magnetic field. [S1063-651X(99)05707-4]

PACS number(s): 47.20.Bp, 47.54.+r, 61.30.−v

I. INTRODUCTION

Nematic liquid crystals are fluids with long-range orientational order of their elongated molecules [1]. The anisotropy due to the orientational ordering is reflected in the material parameters such as the viscosity and the thermal conductivity, and in the constitutive equations. Under nonequilibrium conditions the anisotropy effects lead to a rich variety of new pattern-formation phenomena which do not occur in isotropic fluids. With increasing temperature the orientational order of the fluid is reduced until it vanishes *discontinuously* at the nematic-isotropic transition temperature $T_{\rm NI}$. This phase transition to the isotropic phase is of first order; latent heat Q has to be provided, and the density ρ decreases discontinuously by a jump $\Delta\rho$. Numerous recent experimental and theoretical studies of convection in nematic liquid crystals have significantly advanced our understanding of pattern formation in nonequilibrium systems (for reviews, see, for instance, Refs. [2] and [3]).

One of the best-studied paradigms of hydrodynamic pattern-forming systems is Rayleigh-Bénard convection (RBC) [4–6], i.e., convection of a thin horizontal fluid layer heated from below. The quiescent layer becomes unstable and undergoes a transition to buoyancy-driven convection when the temperature difference $\Delta T = T_b - T_t$ across it exceeds a threshold value ΔT_c (T_b and T_t are the temperatures at the bottom and the top of the layer, respectively). RBC in nematics has also been investigated intensively [7–11]. In this case a magnetic field couples to the fluid and can serve as an additional control parameter. This opens up a rich bifurcation diagram which contains many new features not found in convection of isotropic fluids, such as subcritical stationary and oscillatory onset of convection, ''oblique'' and ''abnormal'' rolls, and tricritical and Lifshitz points. Considering the complexities of the equations of motion, the agreement achieved between experiment and theory is remarkable in most cases.

Nematic liquid crystals offer an additional opportunity to study an interesting stability and pattern-formation problem, namely, convection in the presence of a first-order phase change [12–15,7]. This is the topic of the present paper. When the vertical temperature difference ΔT across a convection cell of thickness d straddles $T_{\rm NI}$, an interface between the two phases exists at that vertical position z_0 where the local temperature is equal to $T_{\rm NI}$. Taking the origin of the vertical (z) axis at the bottom of the cell, and measuring length in units of d, the low-temperature (more dense) nematic phase will have a thickness $1-z_0$. It will be stratified *above* the *less dense* isotropic phase. In the absence of a temperature gradient this configuration is unstable in the presence of gravity. Remarkably, heating the system from below can stabilize this adverse density distribution over certain parameter ranges. From experiment it seems that the nematic nature of the upper phase has at most a minor influence on the instability mechanism and the bifurcation lines, although it affects some of the pattern-formation phenomena which occur.

For *isotropic* fluids the problem was examined theoretically by Busse and Schubert [12,5]. They were able to capture several central components of the instability mechanism by a set of approximate equations of motion. The theory includes the usual driving force of convection due to buoyancy associated with the increasing density of the fluid with decreasing temperature from the cell bottom to its top.

In addition, the interface between a more dense layer stratified above a less dense one has the tendency to become unstable due to gravity. A small vertical fluctuation with horizontal wave number p of the interface position will create a fluid column of width π/p with a relatively large average density adjacent to a similar column of lesser average density, making it favorable for the heavy column to sink and the lighter one to rise. The corresponding Rayleigh-Taylor instability was studied extensively in the past for two immiscible phases of distinct fluids [16]. However, often temperature gradients were omitted or buoyancy was neglected. Such an analysis is thus expected to be relevant to our experiments in the presence of a *vanishingly small* temperature gradient, when ΔT is just large enough to straddle the transition temperature. The situation is qualitatively different for *large* temperature gradients. They will tend to suppress the amplitudes of spontaneous interface fluctuations because the interface essentially is restrained to be located at that precisely defined vertical position where the local temperature equals the transition temperature. The interface is actually *stabilized* in this case. Finally, the effect of the latent heat at the interface, which does not exist in the Rayleigh-Taylor problem, must be considered. The detailed theoretical analysis [12] is consistent with the qualitative conclusion that a local fluctuation in the upward mass transport (velocity) through the interface (driven perhaps by an interface fluctuation as described above) will require the conversion of isotropic to nematic fluid, and thus will release heat. This leads to local heating in the neighborhood of the fluctuation, thereby creating an additional positive buoyancy force. Similarly, a downward velocity fluctuation will absorb heat, producing cooling in its vicinity and thus enhancing the negative buoyancy which prevails there. However, intuitive reasoning of this kind has to be taken with caution, since it also led to the opposite (incorrect) conclusion, namely, that latent-heat effects would be stabilizing [17]. One also has to keep in mind that the consideration of the buoyant forces alone is insufficient. As in classical RBC, the destabilization of the quiescent state requires in addition that the dissipative forces (viscosity, heat diffusion) can be overcome. In the end the interaction of all these effects makes it possible over some parameter ranges for a more dense phase to be stably stratified above a less dense one.

The theoretical work of Busse and Schubert [12] was motivated by the relevance of the interface instability to geophysical and astrophysical problems. The stability of a dense phase above a less dense one plays a role in geothermal situations, where, for instance, water can be stably stratified above steam. [5,17] Phase changes also are important for convection in the Earth's mantle [18] and in stars. However, in these latter cases there are very large gravitational pressure gradients, and it is believed that the more dense phase is located below the less dense one. An instability can occur nonetheless because the latent heat which is released by an interface displacement can still destabilize the system. Various types of interface instabilities, including ones with negative latent heat [19] and when heating from above, were enumerated by Busse [5]. Most of them are not readily achieved in the laboratory. We believe that the semiquantitative agreement between experiment and theory which we report for the case under examination here strengthens the case for applying the theory to the experimentally less accessible ones.

There have been only qualitative experiments relevant to this interesting system [13,14] until very recently [15]. The first experimental investigation of which we are aware was by Fitzjarrald [13], who used the same nematic liquid crystal as the one employed in the present investigation. He heated from below as in our work, but did not apply a magnetic field. The results of this research are qualitative. Neither threshold values ΔT_c nor critical wave numbers α_c for the onset of convection were given. The work did not reveal that there are *two* separate re-entrant conduction regimes, one at small and the other at large z_0, and that the patterns for z_0 near $\frac{1}{2}$ consist of rolls (see Sec. V B below). However, in agreement with the present work, the author also identified two types of cellular patterns, distinguished by having upflow or downflow at the cell centers.

The experiments of Salan and Guyon [14] were designed primarily to study convection in a homeotropically aligned nematic liquid crystal [methoxybenzylidene *p*-(*n*-butyl)aniline or MBBA] in a vertical magnetic field and heated from above. For a relatively large field, convection began only when the temperature difference was quite large and hexagons occurred due to the non-Boussinesq nature of the sample. At even larger ΔT, the nematic-isotropic transition temperature T_{NI} was reached at the top of the sample. At first hexagons continued to exist, but when the top temperature was so large as to create a continuous isotropic layer, the pattern consisted of disordered rolls which tended to terminate with their axes orthogonal to the cell wall in a manner similar to the patterns of isotropic fluids.

In Ref. [15] significant information about the parameter ranges for various types of patterns as well as quantitative results for the bifurcation lines were reported. However, in that work the top temperature was held fixed and only the bottom temperature was varied. This procedure is easier experimentally than one in which the interface position is held fixed, but it leads to a complicated experimental path for a given run in which the interface first forms at the bottom and then gradually moves towards the top as ΔT is increased. Some ranges of the relevant parameter space were difficult to reach and were not explored. Nonetheless, where comparison is possible, the results reported in the present paper are generally consistent with that work, although there are some differences in detail with regard to the parameter ranges over which certain patterns are found. These differences presumably are attributable to the bistability associated with subcritical or transcritical bifurcations, although this has not been investigated more closely. There is one issue on which our present understanding differs from the conclusions drawn in Ref. [15]. On the basis of the bifurcation points measured along the complicated experimental paths of that work, it was concluded erroneously that there are two codimension-2 points in this system where two-phase-convection bifurcation lines cross Rayleigh-Bénard bifurcation lines. It is now clear that one goes smoothly over into the other, and that there is no point in parameter space where two distinct primary bifurcation lines meet.

Here we report quantitative measurements of heat transport in the form of Nusselt numbers which enabled us to determine the stability boundaries $\Delta T_c(z_0)$ of the quiescent

state in the ΔT-z_0 plane with good accuracy. In these experiments, the top and bottom temperatures were adjusted independently so as to keep the interface position z_0 constant as ΔT was varied. This experimental path facilitates comparison with the theory. We also calculated the bifurcation lines, using the equations of motion proposed by Busse and Schubert [12], with an additional term which provides the effect of the interface tension. Using the fluid properties of our system, we found quite good agreement between the theory and the experiment.

We present results for the convection patterns which form in various regions of the ΔT-z_0 plane. It turns out that two-phase convection involves interesting nonlinear problems, such as the exchange of stability between hexagons and rolls. A great diversity of patterns is observed in the convecting states, including near-perfect parallel rolls, rolls with defects and curvature, and cellular flow with upflow or downflow at the cell center. To a large extent the parameter ranges over which these patterns occur can be understood qualitatively in terms of the breaking of the mirror symmetry at the horizontal midplane of the cell by the interface, and in terms of the magnetic-field effects on the nematic phase.

From some of the convection patterns near onset we determined approximate values of wave numbers. For comparison, we calculated the critical wave numbers from the equations of motion. Here the experiment and the agreement with theory is only semiquantitative. One reason for this may be that it is difficult to reach a true steady state in some parameter regions because the approach to it is extremely slow. Thus the patterns often remained somewhat disordered, and from our Fourier analysis we may have obtained a wave number which is too small. Another reason may be that the bifurcations are expected to be subcritical or transcritical. In that case the experiment near onset yields the wave number of a finite-amplitude state whereas the theory corresponds to infinitesimal critical perturbations of the conduction state. Some of the results reported in the present paper have been summarized briefly in a recent review [7].

II. APPARATUS, SAMPLE, AND EXPERIMENTAL METHODS

The apparatus used by us was described in detail elsewhere [8,15,7,20]. It was a standard Rayleigh-Bénard convection apparatus with optical access from above which was designed for the study of convection in liquids at ambient pressure. Its special feature was that it was made entirely of nonmagnetic materials. It was located in the 19.5-cm gap between specially shaped pole pieces of a Varian electromagnet which provided a horizontal magnetic field of magnitude H with a uniformity of ± 0.1 % over a sample diameter of up to approximately 5 cm. The sample of circular cross section was located inside a ''can'' in a water bath. The top of the sample was a sapphire which was exposed on the outside to temperature-controlled circulating water. The temperature stability of the water was better than 1 mK. The sample was confined by an aluminum bottom plate which could be heated from below by a metal-film heater. The thickness of the cell was $d=0.327$ cm, and the aspect (radius to thickness) ratio was $\Gamma=12.7$. The present work was carried out for $H=1000$ G. Images of the convection patterns were acquired by a computer-interfaced camera from diffuse scattering of ambient light by the nematic phase.

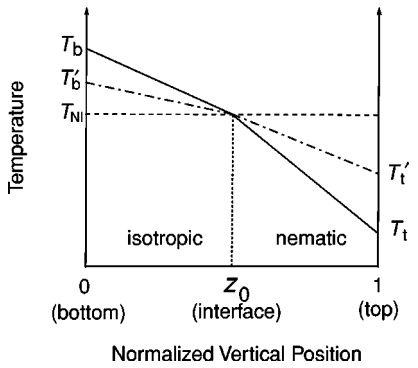

FIG. 1. Schematic diagram of temperature profiles in the conduction state. The dash-dotted line corresponds to a smaller heat current, and the solid line to a larger heat current, at fixed z_0.

The sample was 4−n−pentyl−4'−cyanobiphenyl (5CB) [21], with a nematic-to-isotropic transition temperature $T_{\rm NI}$ in the range 35.2–34.9 °C. We determined $T_{\rm NI}$ at various times during this project with a resolution of about 10^{-2} °C by evaluating the brightness of images at various temperatures incremented in steps of 5 mK. There was no hysteresis in the brightness with increasing and decreasing temperature. It was found that $T_{\rm NI}$ gradually decreased with time, on average by 2.65 mK/day in the initial stage (0–70 days after a new cell was filled) and by 1.55 mK/day in the later stages of the project (70–170 days). This monotonic time dependence of $T_{\rm NI}$ may perhaps be attributed to a small amount of contamination leached out of the O ring and delrin cell wall used for sealing the sample fluid. Although the decay of $T_{\rm NI}$ was quite small within an experimental run (typically a couple of days), even a very small uncertainty in $T_{\rm NI}$ causes a significant error in the estimate of the interface position when the temperature difference ΔT across the cell is small. Therefore, we used a time dependent $T_{\rm NI}$ for the determination of the interface position z_0 in every experimental run.

Typical temperature profiles in the sample cell are shown schematically in Fig. 1 for two values of ΔT. Since the conductivity in the lower isotropic phase is larger than that in the upper nematic phase [20], the temperature gradient was smaller in the lower phase than in the upper one. The interface position is given by

$$z_0=I_I/(I_I+I_N), \tag{2.1}$$

where

$$I_I=\int_{T_b}^{T_{\rm NI}}\lambda_I dT, \quad I_N=\int_{T_{\rm NI}}^{T_t}\lambda_N dT. \tag{2.2}$$

Here the conductivities λ_I and λ_N are for the isotropic and nematic phases, respectively. Because of the large applied horizontal field, the relevant conductivity of the nematic phase is $\lambda_N=\lambda_\perp$. Both $\lambda_\perp$ and λ_I are known quantitatively [20]. They can be represented by

$$\lambda=\lambda_0+\lambda_1\ (T-T_{\rm NI})+\lambda_s, \tag{2.3}$$

where λ_s is a singular contribution. Below $T_{\rm NI}$,

$$\lambda_{s,\perp}=\lambda_{1,\perp}\ (T_c-T)^{\alpha_\perp}. \tag{2.4}$$

In the isotropic phase, λ_s vanishes. The parameters needed are $\lambda_0=1.512\times10^4$, $\lambda_1=-37.0$, $\lambda_{1,\perp}=-1.448\times10^3$, $T_c=36.06$ °C, and $\alpha_\perp=0.172$. Here λ has the units erg/s cm K. The results for λ can be used to evaluate z_0 from Eq. (2.1). As $\Delta T=T_b-T_t$ was changed in a given experimental run, T_b and T_t were changed in such a way as to hold z_0 constant.

The effective conductivity of the sample was evaluated using

$$\lambda_{\rm eff}=\tilde{Q}d/(A\Delta T), \tag{2.5}$$

where $\tilde{Q}$ is the heat current passing through the sample (after correction for the current carried by the cell walls) and $A=\Gamma^2d^2\pi$ is the area of the sample. The Nusselt number N is the ratio

$$N=\lambda_{\rm eff}/\lambda_{\rm eff,0} \tag{2.6}$$

where $\lambda_{\rm eff,0}$ is the average conductivity of the quiescent fluid given by

$$\lambda_{\rm eff,0}=(I_N+I_I)/(T_b-T_t). \tag{2.7}$$

III. THEORETICAL ANALYSIS

In this section our theoretical analysis for the onset of convection, based on the (slightly generalized) Busse-Schubert equations of motions [12], is described briefly. All details, like the scaling conventions or the explicit form of the parameters, are explained in the Appendix.

The equations are

$$\frac{\kappa}{\nu}\nabla^2\frac{\partial f}{\partial t}=\nabla^4 f-\left[P\left(1+\sigma\frac{\partial^2}{\partial x^2}\right)\delta(z-z_0)+1\right]\theta, \tag{3.1}$$

$$[1+R_\beta\delta(z-z_0)]\frac{\partial\theta}{\partial t}=\nabla^2\theta-[R_Q\delta(z-z_0)+R]\frac{\partial^2}{\partial x^2}f, \tag{3.2}$$

where κ is the thermal diffusivity, ν the kinematic viscosity, and σ the dimensionless surface tension. They couple the velocity potential f and the deviations θ of the temperature from the conduction profile, which both begin to grow exponentially at threshold. Besides the familiar Rayleigh number R, we introduce the additional control parameters $R_{\Delta\rho}$ and R_Q, which characterize the interfacial Rayleigh-Taylor instability and the destabilization by the latent-heat effects, respectively. They are related to the parameters P and R_β defined in Ref. [12] and used in Eqs. (3.1) and (3.2) by $P=R_{\Delta\rho}/R$ and $R_\beta=R_Q/R$.

A central result of Ref. [12] was that the increase of any of the three control parameters separately drives the quiescent system towards instability. The analytical considerations of Ref. [12], made possible for certain limiting cases and approximate free-slip boundary conditions, have proven to be illuminating in reaching that conclusion. We consider the results of Ref. [12] for zero surface tension and for $R_Q,R_\beta\to0$. It turns out that the Rayleigh-Taylor instability takes place only for P above a certain (large) threshold. For fixed $\Delta\rho$ this requires ΔT to be very small, whereas in the presence of a finite temperature difference the instability is suppressed. One can also see from Eq. (3.1) that a finite surface tension σ tends to reduce the prefactor of the δ function on the right-hand side, and thus the tendency toward the Rayleigh-Taylor instability. Further, by considering the opposite limit of dominant buoyancy ($R_{\Delta\rho},R_Q\ll R$), it was demonstrated in Ref. [12] that the critical Rayleigh number decreases with increasing $R_{\Delta\rho}$ and R_Q, i.e., again the destabilization due to two-phase effects became evident. Since the analysis of Ref. [12] covered neither the present experimental parameters nor the realistic rigid boundaries and the case of finite surface tension σ, we determined the onset of convection numerically from the above equations, as explained in the Appendix.

IV. EXPECTED PATTERNS

Here we consider qualitatively the patterns that are to be expected in this system. In the framework of the weakly nonlinear stability analysis [22] it is well understood why roll patterns characterized by a single wave vector typically occur in many systems. Cellular patterns, however, require the resonant interaction of degenerate or nearly degenerate modes with different wave vectors. For this to happen, the mirror symmetry at the horizontal midplane of the cell has to be broken. Well known examples are the hexagonal planforms in isotropic fluids [23] which are associated with non-Boussinesq effects, i.e., with significant variations of the material parameters throughout the cell because of the imposed temperature gradient. The bifurcation is then transcritical. The cells have upflow (downflow) at their centers when the various properties like the viscosity and the thermal conductivity decrease (increase) with temperature. Upflow (downflow) is realized in most liquids (gases).

The present system differs in several important aspects from isotropic fluids. The mirror symmetry is always broken by the existence of an interface which separates the two layers with different material parameters. When cellular flow occurs, we believe that the flow direction at the cell centers depends on whether the interface is located significantly above or below the midplane. When the interface is located near the midplane, the symmetry breaking is relatively mild and it turns out that rolls can still exist.

An additional feature is that the system is anisotropic, particularly in the presence of a strong horizontal magnetic field $\vec{H}$. The ''director'' **n**, which describes the orientational degrees of freedom of the nematic, tends to align parallel to $\vec{H}$. In RBC of a *single-phase* nematic layer with thickness d the pattern-formation phenomena [8,7,24] are controlled by the value of the dimensionless field

$$h=H/H_F, \tag{4.1}$$

where the Fréedericksz field H_F is given by

$$H_F=\frac{\pi}{d}\sqrt{\frac{k_{11}}{\rho\chi_a}}. \tag{4.2}$$

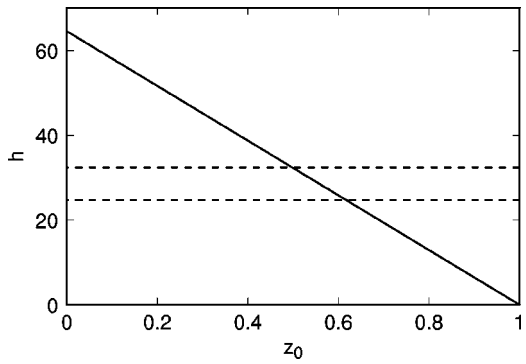

FIG. 2. Schematic diagram of the dimensionless field h as a function of the isotropic layer thickness z_0. The two dashed horizontal lines are the two Lifshitz fields h_{L1} and h_{L2} (see text) with parallel rolls at smaller and longitudinal rolls at larger z_0.

Here k_{11} is one of the elastic constants, ρ is the density, and χ_a is the anisotropy of the diamagnetic susceptibility. When $h>h_{L2}\simeq 32.4$, convection rolls will form with their axes parallel to $\vec{H}$. For $h<h_{L1}\simeq 24.7$, normal rolls (convection rolls with their axes perpendicular to $\vec{H}$) will develop. As the field increases from h_{L1} to h_{L2}, oblique rolls exist and the roll axis continuously changes with H from the normal to the parallel orientation. As a guide to the patterns which might be expected in the two-phase system, we assume that the patterns are approximately consistent with the thickness of the nematic phase and the known behavior of the single-phase nematic system. The layer thickness d in Eq. (4.2) must then be replaced by $d(1-z_0)$, and

$$h=\frac{d(1-z_0)}{\pi}\sqrt{\frac{\rho\chi_a}{k_{11}}}H. \tag{4.3}$$

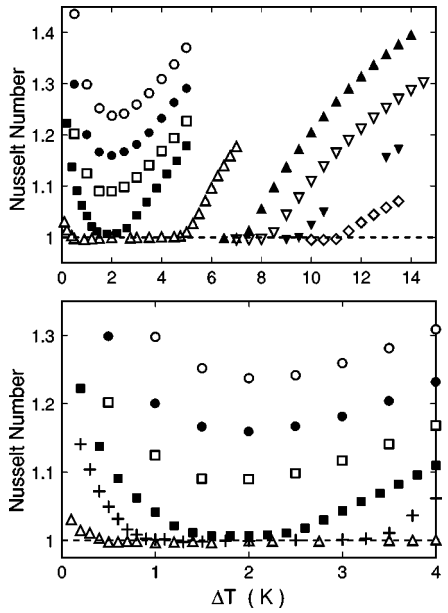

FIG. 3. Nusselt numbers as a function of the temperature difference ΔT across the cell for various interface positions $z_0<0.45$. For clarity, only some of the data are shown. ○: $z_0=0.43$. ●: $z_0=0.32$. □: $z_0=0.27$. ■: $z_0=0.24$. +: $z_0=0.22$. △: $z_0=0.17$. ▲: $z_0=0.00$. ▽: $z_0=-0.10$. ▼: $z_0=-0.20$. ◇: $z_0=-0.29$.

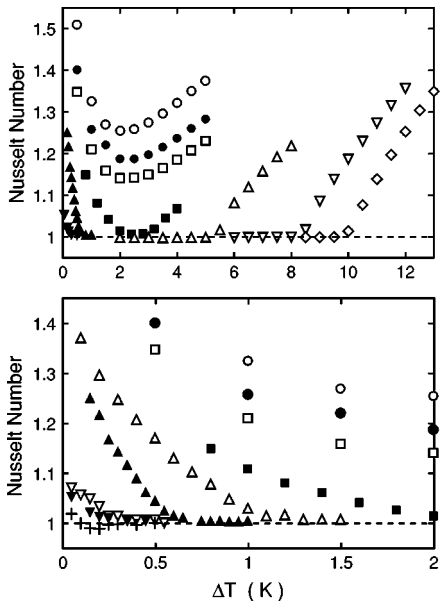

FIG. 4. Nusselt numbers as a function of the temperature difference ΔT across the cell for various interface positions $z_0>0.45$. For clarity, only some of the data are shown. ○: $z_0=0.48$. ●: $z_0=0.58$. □: $z_0=0.63$. ■: $z_0=0.69$. △: $z_0=0.72$. ▲: $z_0=0.77$. ▽: $z_0=0.82$. ▼: $z_0=0.86$. +: $z_0=0.91$. ◇: $z_0=1.00$.

This function, evaluated for the fluid properties of the nematic phase [25] just below $T_{\rm NI}$ and our d and H, is shown in Fig. 2 as a function of z_0. Also shown as horizontal dashed lines are h_{L1} and h_{L2}. One sees that, if rolls are the preferred planform, they should be parallel to the field if $z_0\lesssim 0.5$. For $z_0\gtrsim 0.6$, one would expect rolls to form with their axes orthogonal to $\vec{H}$. Of course, as discussed above, there will be large parameter ranges, particularly for z_0 close to zero and z_0 close to 1, over which rolls do not form at all, and where cellular or hexagonal planforms dominate.

V. RESULTS

A. Nusselt numbers and bifurcation lines

Results of Nusselt-number measurements along several paths of constant vertical interface position z_0 are shown in Figs. 3 and 4. Here Fig. 3 is for the smaller and Fig. 4 for the larger values of z_0. In both cases, the upper figure covers a broad range of the z_0-ΔT space, and the lower one is an enlargement of the region near $z_0=0$ or $z_0=1$.

For $0<z_0\lesssim 0.24$ and $0.70\lesssim z_0<1$, the data reveal directly the re-entrant nature of the instability. Over these ranges, there is convection ($N>1$) *below* a critical value ΔT_1, as well as above a second larger value ΔT_2. For the intermediate range $0.24\lesssim z_0\lesssim 0.70$ convection occurs for *all* temperature differences, but N initially decreases with increasing ΔT, consistent with a stabilizing influence of the temperature gradient. The results for N yield values of ΔT_1 and ΔT_2 which are shown in Fig. 5 as solid circles.

Also shown in Fig. 5, as solid and dashed lines, are the results of the linear stability analysis described in Sec. III and the Appendix. We found only stationary bifurcations at threshold, over the entire parameter range. A vanishing of θ at the interface, which would correspond to separated con-

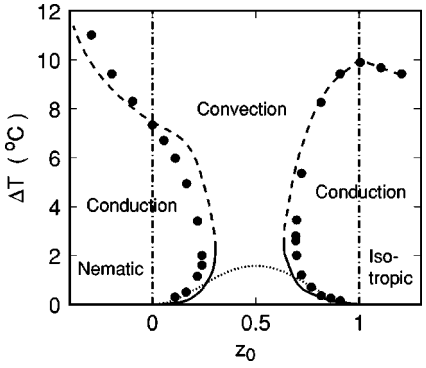

FIG. 5. Stability boundaries in the z_0-ΔT plane. The solid circles are the experimentally determined values. The solid (dashed) lines are the results of the calculations for the lower (upper) branches of the re-entrant bifurcation lines. The dotted line corresponds to the case $R_Q, R_\beta \to 0$ which was evaluated analytically in Ref. [12]. The dash-dotted lines indicate the limits of the two-phase region.

vection rolls in the two phases [12], never occurred. As in the experiment, the calculation also yields reentrant conduction with two values of a critical ΔT when z_0 is sufficiently small or large. In the theory, the reentrant regions extend over the ranges $0 < z_0 \lesssim 0.30$ and $0.64 \lesssim z_0 < 1$, which are about 20 % wider than the ranges found by experiment. Considering the approximations which were involved in the theoretical analysis (see the Appendix), we find the agreement with experiment very satisfactory. A likely significant contribution to the small differences is the assumption of constant and equal properties for the two phases (except for ρ), since it is known that particularly the properties of the nematic phase vary considerably with temperature near T_{NI} [7].

Also shown (as a dotted line) in Fig. 5 is the limiting case $R_Q, R_\beta \to 0$ which was evaluated analytically in Ref. [12]. In this approximation convection occurs only below the line, and the conduction state extends to arbitrarily large ΔT above it.

B. Patterns

The typical patterns which were found at various values of z_0 and ΔT are illustrated in Figs. 6–10. For all of the images, a magnetic field of 1000 G is in the horizontal direction. Each figure shows four images, and below them the Nusselt-number results for the particular value of z_0. In the plots of N vs ΔT, the points corresponding to the four images are identified. Although there is little experimental information about the nature of the bifurcations, some or many of them presumably are transcritical or subcritical. Thus there may well be bistability, and the patterns shown here for a particular point in parameter space may not be unique.

In Figs. 6, 9, and 10 the Nusselt number again reflects the reentrant nature of the instability. For $z_0 = 0.17$ (Fig. 6) and $z_0 = 0.86$ (Fig. 10), image (c) does not reveal any structure, consistent with the quiescent state suggested by the result $N \simeq 1$. For $z_0 = 0.72$ (Fig. 9), a faint roll structure is noticeable for image (c), even though the measurements of N suggest that this image is located in the reentrant conduction region. We believe this to be associated with the extreme

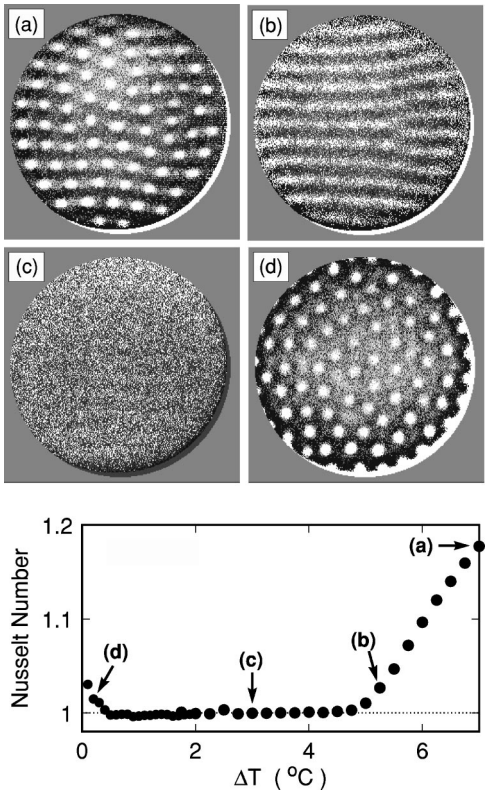

FIG. 6. Nusselt numbers and patterns for $z_0 = 0.17$. Images (a), (b), (c), and (d) correspond to the Nusselt-number points identified by arrows in the graph.

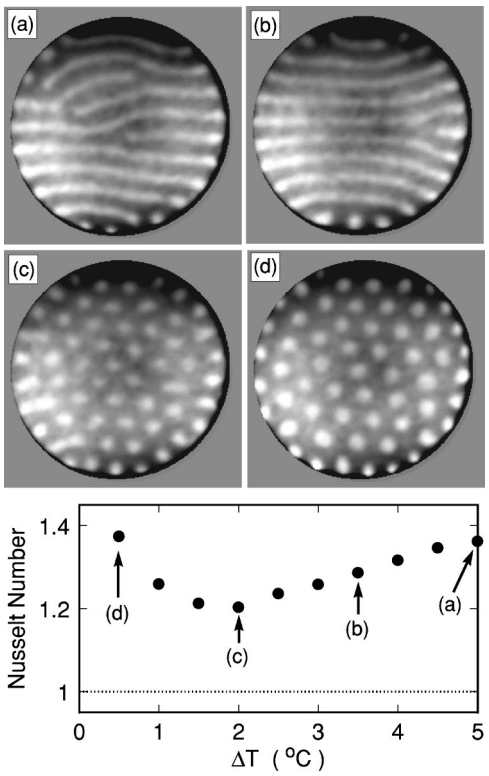

FIG. 7. Nusselt numbers and patterns for $z_0 = 0.38$. Images (a), (b), (c), and (d) correspond to the Nusselt-number points identified by arrows in the graph.

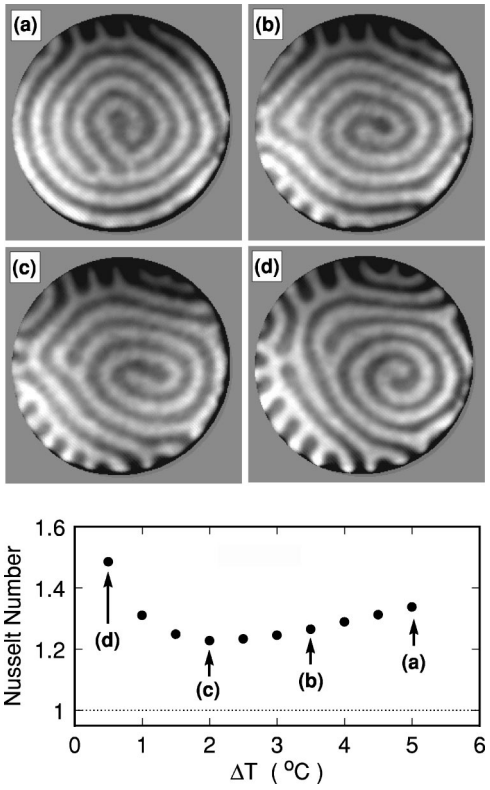

FIG. 8. Nusselt numbers and patterns for $z_0 = 0.53$. Images (a), (b), (c), and (d) correspond to the Nusselt-number points identified by arrows in the graph.

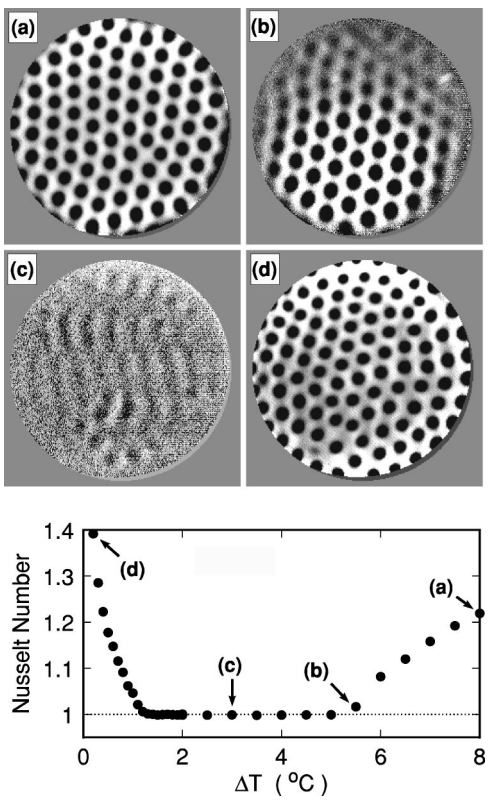

FIG. 9. Nusselt numbers and patterns for $z_0 = 0.72$. Images (a), (b), (c), and (d) correspond to the Nusselt-number points identified by arrows in the graph.

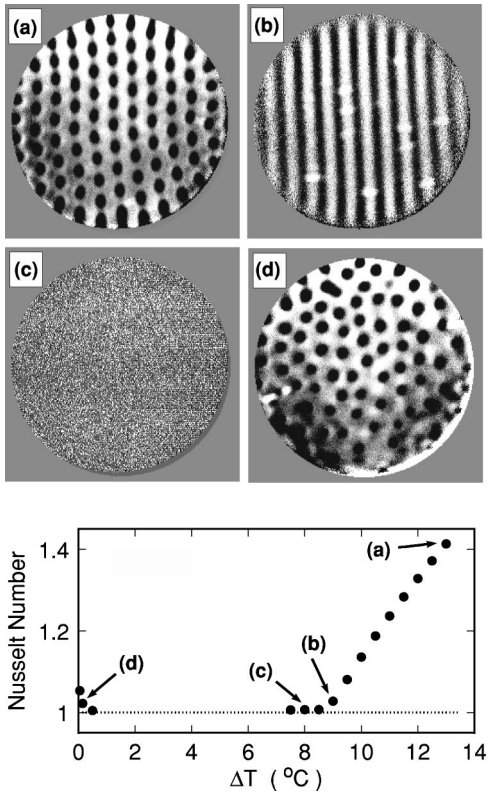

FIG. 10. Nusselt numbers and patterns for $z_0 = 0.86$. Images (a), (b), (c), and (d) correspond to the Nusselt-number points identified by arrows in the graph.

closeness of the near-vertical bifurcation line to this particular experimental path (see Fig. 5).

At small $z_0 = 0.17$ (Fig. 6), the flow at large ΔT [image (a)] is cellular. For this value of z_0 the interface, being near the cell bottom, has a sufficiently strong symmetry-breaking effect to prevent the formation of rolls. The cell centers appear bright, which corresponds to enhanced scattering of ambient light. Unfortunately we have not been able in our experimental setup to measure whether this corresponds to upflow or downflow.

Surprisingly, a reduction of ΔT yields a transition to rolls [image (b)]. The rolls are oriented with their axes parallel to $\vec{H}$, as expected on the basis of Fig. 2 for small z_0. The same orientation is also noticeable in the arrangement of the cellular flow of image (a). The appearance of rolls as ΔT is reduced suggests that the asymmetry due to the interface is weak until convection causes some mixing of the two phases. A secondary bifurcation between the rolls and the cellular flow has not been resolved in the Nusselt-number measurements. Finally, for very small ΔT [image (d)], the flow is cellular again, also with white cell centers. Here the field does not seem to have any ordering effect.

For $z_0 = 0.38$ (Fig. 7), the flow at large ΔT [images (a) and (b)] consists of rolls with some defects, with the dominant orientation still consistent with the high-field region suggested by Fig. 2. Although convection is quite vigorous, there is in this case no suggestion of cellular flow at large ΔT. Apparently the symmetry breaking is weak because the interface is located near the midplane of the cell. There is no re-entrant conduction region, and instead the pattern evolves directly into cellular flow as ΔT is reduced [images (c) and

(d)], with bright centers. In this cellular region any ordering effect from the field is not obvious to the eye.

For $z_0=0.53$ (Fig. 8), the flow is roll-like, but the rolls form a spiral and numerous defects near the wall. Similar patterns were also found, for instance, for $z_0=0.48$, but in that case the rolls tended to form target patterns and numerous defects near the wall. At this value of z_0 we are in the field region between the two Lifshitz fields in Fig. 2, and apparently the orienting effect of h is weak. Cellular patterns were not observed at all, suggesting that the symmetry breaking due to the interface does not play a large role for z_0 near $\frac{1}{2}$.

For $z_0=0.72$ (Fig. 9), the flow is cellular except in the re-entrant conduction region. In contrast to smaller z_0, the cell centers are now black, corresponding to reduced scattering of the ambient light. Presumably the flow direction at the cell centers is opposite to that at small z_0. It is interesting to note that the arrangement of the cells, when they occur, also changes as the interface moves from below to above $z_0\simeq\frac{1}{2}$. For $z_0>\frac{1}{2}$ and above the re-entrant conduction region [images (a) and (b)] the cells are ordered along rows which are orthogonal to the field, consistent with the ordering effect expected from Fig. 2 for field values below the Lifshits fields. At the smaller ΔT [image (d)], there is again no obvious field ordering of the cells.

Finally, for $z_0=0.86$ (Fig. 10), cellular flow occurs at the largest ΔT [image (a)], and a transition to rolls occurs as that ΔT is reduced [image (b)]. This is analogous to the phenomena found for small z_0 (Fig. 6), except for two important differences: consistent with Fig. 2 the roll axes and cells are ordered along lines which are *orthogonal* to the field, and the cell centers are *black*. At small ΔT [image (d)] the field again has little if any ordering effect on the cellular pattern.

C. Wave numbers

In Fig. 11 the critical wave numbers α_c are shown as a function of z_0. Starting at $z_0=0$ and 1, the dashed curves represent the upper branches (compare Fig. 5) which start at the single-phase value $\alpha_c=3.116$ and decrease as z_0 increases beyond 0 or decreases below 1. When the maximum or minimum value of z_0 is reached, α_c decreases further along the lower branches (solid lines), reaches a minimum, and increases as z_0 approaches 0 or 1 again. Thus, $\alpha_c(z_0)$ is double valued.

Using the fact that $P=R_{\Delta\rho}/R$ diverges as $\Delta T\to 0$, one can show from Eq. (3.1) that the critical wave number α_c diverges as z_0^{-1} or $(1-z_0)^{-1}$ as z_0 approaches 0 or 1 [12]. However, a finite interface tension σ is very effective in suppressing short-wavelength spatial variations of the interface, and thus leads to a strongly reduced amplitude of these divergences [26]. Our calculations did not go to sufficiently small or large z_0 to clearly reveal the divergence numerically, but they do show an increase of α_c as $z_0\to 0$ and $z_0\to 1$. For comparison, we show as a dotted line the analytic result of Ref. [12] for $R_\beta, R_Q\to 0$. One sees that the amplitudes of the divergences are much larger in this case.

The experimental determination of α_c was difficult because the patterns near onset often were rather disordered [see, for instance, Figs. 6(d) or 10(d)], because the bifurcations presumably led to finite amplitudes at onset, and because our sample had only a modest aspect ratio where boundaries influenced the pattern. Thus we regard the experimental determinations of α_c only as semi-quantitative. In Fig. 11, data for the lower branches are given as solid circles. For large z_0 they agree rather well with the calculation (solid line). For small z_0 they are 10–20 % lower than the theoretical values, but for the reasons given above we do not regard this as a significant discrepancy. The data would not be consistent with the strong divergences indicated for the case without surface tension in the limit $R_Q, R_\beta\to 0$ (dotted line).

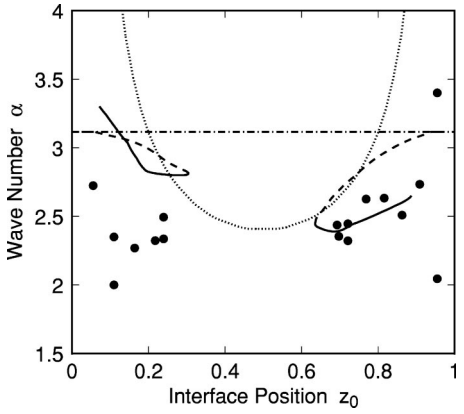

FIG. 11. Critical wave numbers as a function of the interface position z_0. The solid (dashed) lines are the results of the calculations for the lower (upper) branches of the re-entrant bifurcation lines (see Fig. 5). The dotted line corresponds to the case $R_Q, R_\beta \to 0$, which was evaluated analytically in Ref. [12]. The dash-dotted line corresponds to the value 3.116 for the single-phase fluid. The solid circles are experimental estimates along the two lower branches.

VI. SUMMARY AND CONCLUSION

In this paper we presented experimental results and theoretical calculations for convection in a horizontal layer of a fluid with a first-order phase change which is heated from below. In the experiment we used a liquid crystal with a nematic-isotropic transition, under conditions where the temperature difference ΔT extended from below to above the transition temperature $T_{\rm NI}$ so that the more dense nematic phase was stratified above the isotropic one. We applied a magnetic field of 1000 G in order to assure a director alignment parallel to this field. For the theory we carried out a stability analysis of the equations of motion formulated by Busse and Schubert, [12] with the addition of an interface-tension term. Our results for the bifurcation lines based on realistic parameters corresponding to the properties of the fluid used in the experiment, as well as the experimental measurements, are shown in Fig. 5. For sufficiently small but finite ΔT we found both theoretically and experimentally that this system is always unstable to convection. However, the temperature gradient has a stabilizing influence, and for a vertical interface position z_0 sufficiently small or sufficiently large re-entrant stable conduction states were reached as ΔT was increased. For even larger ΔT convection occurred again, due to the usual Rayleigh-Bénard mechanism. The transition from the interface instability at small ΔT to the Rayleigh-Bénard instability at large ΔT was continuous and smooth in the ΔT-z_0 plane. In the re-entrant conduction

states the more dense nematic phase was stably stratified above the less dense isotropic one, as originally predicted by Busse and Schubert [12] for isotropic fluids. Although the general features of the bifurcation diagram in the ΔT-z_0 plane were the same in the theory and the experiment, the maximum widths along the z_0 axis of the conduction states in the theory were about 20% larger than in the experiment. We expect that this difference at the quantitative level is due to approximations made in the calculation, in particular to the assumption that both phases have the same properties except for the density difference. Considering the complexities of this system, we thus regard the general agreement with the experiment as quite satisfactory. We conclude that the Busse-Schubert concept [12] of two-phase convection, when evaluated quantitatively for realistic fluid properties, describes the experiments rather well.

Busse and Schubert derived an analytic result for the bifurcation line for the special case where certain parameters of the problem vanish ($R_Q, R_\beta \to 0$; see Sec. III). They found a re-entrant conduction regime for all z_0, as is shown by the dotted curve in Fig. 5. This case does not capture properly the transition between the interface instability and the Rayleigh-Bénard instability and is similar to the physical system only near $z_0=0$ and $z_0=1$.

We also calculated the critical wave numbers of the instability along the two bifurcation lines and compared them with approximate experimental determinations. These results are shown in Fig. 11 as solid and dashed curves. Here the experimental results are rather uncertain for two reasons. First, the patterns very near the bifurcation equilibrated very slowly in certain parameter ranges and often remained disordered throughout an experimental run, thus yielding excessively small wave numbers. Second, the bifurcations are expected to lead to finite-amplitude convection which may have a wave number which differs from that of the critical infinitesimal perturbations of the theory. For these reasons we do not regard the differences of up to 20% or so between theory and experiment as significant.

We obtained experimental results for the patterns which form in various parameter ranges and report them in Figs. 6–10. Depending on ΔT and z_0, we found near-perfect straight rolls, straight rolls with defects, highly curved rolls, and cellular flow with either upflow or downflow at the cell centers. Qualitatively, the parameter ranges for the various patterns can be understood quite well on the basis of the breaking of the mirror symmetry at the horizontal midplane by the interface, and on the basis of the properties of the nematic phase in the presence of a magnetic field. Quantitative understanding of the patterns would require calculations based on the Busse-Schubert equations supplemented by appropriate nonlinear terms. Such calculations have not yet been carried out. For some parameter ranges they would be near impossible because of the large amplitudes, corresponding to plumes of one phase entering another, which develop immediately at onset.

Clearly, the theoretical treatment of the problem could be improved further. The obvious refinement would be the inclusion of temperature dependent fluid properties which differ in the two phases. Given the present experimental status, we do not feel that this is worthwhile at this time. More interesting would be a nonlinear analysis in the parameter ranges where this might seem fruitful. Further, one might consider including the anisotropic properties of the nematic phase if comparison with experiments in which the director degrees of freedom are not frozen by large magnetic fields is desired. In that case the heat-focusing mechanism can become important and reduce ΔT_c, and even heating from above may lead to instabilities of the nematic phase [27,7].

It would also be interesting to relate the present analysis more closely to geothermal situations where, for instance, water can be stratified stably above steam, [28], or to convection in the Earth's mantle [5]. In the latter case it is believed that the lighter phase is stratified above the heavier one; but an instability can occur nonetheless because of the latent heat released or absorbed during interface fluctuations. This case is difficult to access in the laboratory, but the level of agreement between experiment and theory found in the present work gives confidence in the corresponding theoretical calculations. Similarly, it would be interesting to consider the case of heating from above, both theoretically and experimentally.

ACKNOWLEDGMENTS

The authors would like to thank Professor F. Busse for many illuminating discussions. The work in Santa Barbara was supported by the National Science Foundation through Grant No. DMR94-19168. One of us (S.S.) acknowledges support from the Ministry of Education of Japan. Another of us (G.A.) acknowledges support through NATO Grant No. CRG.LG973103.

APPENDIX

In this appendix the (slightly generalized) Busse-Schubert equations [12] are rederived in a manner which follows more closely the conventional treatment of convection including a phase change (see, e.g., Refs. [29–31]). The approximations involved are clearly spelled out and it will become evident how the present calculations might be refined.

It is convenient at first to keep all variables in physical units. A Cartesian coordinate system with the gravitational acceleration g in the negative-z direction is used. The fluid is sandwiched between two plates [parallel to the (x,y) plane] at $z=0$ and at $z=d$, where the temperatures T_b and $T_t<T_b$ respectively are applied. When $T_b \geqslant T_{\rm NI} \geqslant T_t$, a stable superposition of a nematic fluid layer (characterized by an index t or 2) above an isotropic one (index b or 1) can be achieved. For the location z_0 of the resulting flat interface between the two fluids we make the following approximation, which holds with an accuracy of about 10% [see Eq. (2.1), with $\lambda_I=\lambda_N$]:

$$z_0 \simeq d(T_b - T_{\rm NI})/(T_b - T_t). \tag{A1}$$

In the following we deal exclusively with the linear regime. In either layer, the onset of convection is determined by the Boussinesq equations

$$\frac{\partial}{\partial t}\mathbf{v} = -\rho^{-1}\boldsymbol{\nabla}\pi + \hat{\mathbf{z}}\alpha g\,\theta + \nu\boldsymbol{\nabla}^2\mathbf{v}, \tag{A2a}$$

$$\frac{\partial}{\partial t}\theta = +\beta w + \kappa \nabla^2 \theta. \tag{A2b}$$

Here $\mathbf{v}=(u,v,w)$ denotes the velocity field, π is the deviation from the hydrostatic pressure of the quiescent fluid, and θ is the deviation from the static temperature field with the gradient $-\beta$. We assume incompressibility, i.e., $\nabla \cdot \mathbf{v}=0$. Realistic rigid boundary conditions are applied, according to which θ,$\mathbf{v}$, and $\partial w/\partial z$ vanish at $z=0$ and $z=d$. Note that the thermal diffusivity $\kappa \equiv \lambda/\rho C_P$, the thermal expansion coefficient α, the density ρ, the kinematic viscosity ν, as well as β are in principle different in both layers. In the spirit of the Boussinesq approximation their values are determined by an average over each layer. For the specific heat at constant pressure C_P we neglected the singular part which exists below T_{NI}.

It is sufficient to concentrate on roll-like solutions, without variations in the y direction (i.e., $v=0$). Let $\eta(x,t)$ parametrize the position $z=z_0+\eta(x,t)$ of the disturbed interface where certain jump conditions [29,30,32] have to be fulfilled. We recall these conditions here for convenience since they are somewhat scattered in the literature. In the linear regime they can be formulated with respect to the originally flat interface, i.e., in the following the fields $\mathbf{v}$ and θ, as well as their normal ($\|z$) and tangential ($\|x$) derivatives, are understood to be taken at $z=z_0$. From continuity of mass transfer one has at the linear level

$$\rho_2\left(w_2-\frac{\partial \eta}{\partial t}\right)-\rho_1\left(w_1-\frac{\partial \eta}{\partial t}\right)=0. \tag{A3}$$

Note that the velocity w perpendicular to the interface and the velocity of the interface $\partial \eta/\partial t$ must not be identical as for immiscible fluids. From momentum conservation tangential to the interface one obtains

$$\rho_2\left(w_2-\frac{\partial \eta}{\partial t}\right)u_2-\rho_1\left(w_1-\frac{\partial \eta}{\partial t}\right)u_1=(\tau_x)_1-(\tau_x)_2, \tag{A4}$$

where the tangential component of the stress tensor is given as

$$(\tau_x)_i=\mu_i\left(\frac{\partial w_i}{\partial x}+\frac{\partial u_i}{\partial z}\right),$$

with the dynamical viscosities $\mu_i=\nu_i\rho_i$ $(i=1,2)$. In principle one should include tangential variations of the surface tension σ in Eq. (A4), which govern the Marangoni instability in the case of a free surface [32–34]. We have checked explicitly that this mechanism is totally negligible in the present context. Momentum conservation perpendicular to the interface is expressed by

$$\rho_2\left(w_2-\frac{\partial \eta}{\partial t}\right)w_2-\rho_1\left(w_1-\frac{\partial \eta}{\partial t}\right)w_1 = (\tau_z)_2-(\tau_z)_1+\pi_1-\pi_2+(\rho_2-\rho_1)g\eta+\sigma\frac{\partial^2 \eta}{\partial x^2} \tag{A5}$$

with the normal component of the stress tensor

$$(\tau_z)_i=2\mu_i\frac{\partial w_i}{\partial z}.$$

Note that the component u of the velocity parallel to the interface as well as any derivative of the fields with respect to the horizontal coordinate x are continuous. Thus the pressure difference can be eliminated with the help of Eq. (A2a),

$$\frac{\partial^2(\pi_2-\pi_1)}{\partial x^2}=\left(\frac{\partial^2}{\partial x^2}+\frac{\partial^2}{\partial z^2}\right)\left(\mu_2\frac{\partial u_2}{\partial x}-\mu_1\frac{\partial u_1}{\partial x}\right). \tag{A6}$$

It is convenient to implement incompressibility, $\nabla \cdot \mathbf{v}=0$ by the use of a velocity potential $f(x,z,t)$,

$$u=\frac{\partial^2 f}{\partial x \partial z}, \quad w=-\frac{\partial^2 f}{\partial x^2}. \tag{A7}$$

Finally, the balance of thermal energy including the work done by pressure involves the balance of the heat currents and the flow of the enthalpy h through the interface

$$\rho_2\left(v_2-\frac{\partial \eta}{\partial t}\right)h_2-\rho_1\left(v_1-\frac{\partial \eta}{\partial t}\right)h_1=-\left(\kappa_1\frac{\partial \theta_1}{\partial z}-\kappa_2\frac{\partial \theta_2}{\partial z}\right). \tag{A8}$$

In the following we will discuss the various approximations employed in Ref. [12]. All of them can in principle be avoided at the expense of massive numerical calculations and of physical transparency. In view of the present experimental accuracy and the fact that the deviations from rigorous calculations are estimated to be of the order of 10%, we consider the simplifications of Ref. [12] to be satisfactory for the present. The approximation $\rho_1=\rho_2$ is used implicitly in Eq. (A3). It applies well to our case since $2(\rho_2-\rho_1)/(\rho_1+\rho_2)=O(10^{-3})$. Instead of the different ρ_i, $i=1$ and 2, in both layers we use a weighted average $\overline{\rho}=[(d-z_0)\rho_2+z_0\rho_1]/d$. Consequently one has *continuity of the velocity* perpendicular to the interface, i.e., $w_1=w_2$, which implies together with the continuity of u the *continuity of f and $\partial f/\partial z$* [see Eq. (A7)]. In Ref. [12] the approximation $\mu_1=\mu_2$ was used, which involves an error of the order of 10% $[2(\mu_1-\mu_2)/(\mu_1+\mu_2)=O(10^{-1})]$. Instead of different μ_i, $i=1$ and 2 again their weighted average $\overline{\mu}$ which deviates from the μ_i less then 5% is used. From Eqs. (A4) and (A7), one obtains immediately *continuity of* $\partial^2 f/\partial z^2$. It is now easy to see that, with the approximations used before, the continuity of normal stress equation (A5) together with Eqs. (A6) and (A7), leads to a *discontinuity* in the third derivative of f with respect to z according to

$$\overline{\mu}(\partial^3 f_1/\partial z^3-\partial^3 f_2/\partial z^3)=\left[(\rho_2-\rho_1)g+\sigma\frac{\partial^2}{\partial x^2}\right]\eta. \tag{A9}$$

In the thermal jump condition Eq. (A8) again a weighted average $\overline{\lambda}$ instead of different thermal conductivities λ_i, $i=1$ and 2, is used, which introduces an error of the order of 10%. One arrives at

$$\overline{\rho}\left(w_1-\frac{\partial\eta}{\partial t}\right)Q=\overline{\lambda}\left(\frac{\partial\theta_1}{\partial z}-\frac{\partial\theta_2}{\partial z}\right), \tag{A10}$$

with the latent heat $Q=h_2-h_1>0$ released at the transformation from the isotropic to the nematic phase.

The last step, and perhaps the most subtle one, is to construct an expression for η. One familiar starting point (also used in Ref. [12]) is the assumption of local thermal equilibrium and thermodynamic equilibrium at the deformed interface, i.e., continuity of the temperature and the chemical potential ψ. The static solution is characterized by equilibrium temperature and pressure profiles $T_0(z)$, $\Pi_0(z)$, respectively. At the phase boundary ($z=z_0$) the difference $g(T,P)=\psi_1-\psi_2$ of the chemical potentials of the two phases vanishes. Onset of convection yields a slightly deformed interface ($\eta\neq 0$) and one has small disturbances π,θ superimposed onto the static solution. From the resulting condition

$$g(T_0(z_0+\eta)+\theta(z_0+\eta),\Pi_0(z_0+\eta)+\pi(z_0+\eta))=0, \tag{A11}$$

the excursion η of the interface is determined by a Taylor expansion up to first order with respect to the small quantities η, π,θ:

$$\left(\frac{\partial g}{\partial T_0}\frac{dT_0}{dz}+\frac{\partial g}{\partial\Pi_0}\frac{d\Pi_0}{dz}\right)\eta+\frac{\partial g}{\partial T_0}\theta(z_0)+\frac{\partial g}{\partial\Pi_0}\pi(z_0)=0 \tag{A12}$$

where all derivatives are taken at the interface. In our case the derivative of g with respect to Π_0 can be neglected relative to that of g with respect to T_0. This can easily be checked for the two summands of the factor of η on the left-hand side of Eq. (A12). Their ratio is determined by the slope $(d\Pi_0/dT_0)_c$ of the coexistence (Clausius-Clapeyron) curve evaluated at z_0:

$$\frac{-\partial g/\partial T_0}{\partial g/\partial\Pi_0}=\left(\frac{d\Pi_0}{dT_0}\right)_c=\frac{Q\overline{\rho^2}}{T_0(\rho_2-\rho_1)}. \tag{A13}$$

With the use of $dT_0/dz=(T_2-T_1)/d$ and $-d\Pi_0/dz=(\overline{\rho g})^{-1}$ one finds the ratio of the pressure to the temperature part to be $O(10^{-8})$. A similar estimate holds for the $\pi(z_0)$ term in comparison to the $\theta(z_0)$ one (see also the related discussion in Ref. [12]). Thus we arrive at the simple relation

$$\eta=-\theta(z_0)dT_0/dz=\beta\theta(z_0),\quad \beta=(T_1-T_2)/d. \tag{A14}$$

Note that the reasoning above implies the continuity of θ. Again we have neglected the difference of thermal conductivities in the two phases. Equation (A14) allows for an obvious interpretation: Thermal fluctuations $\theta(z_0)$ lead to an excursion of the originally flat interface compatible with the external temperature gradient.

In Ref. [35] (related to the problem of a possible interface instability for a heavier phase *below* a lighter one, without buoyancy effects) it was pointed out that the requirement of thermodynamic equilibrium is in principle questionable: Thermal equilibrium can in general only be reconciled with thermodynamic equilibrium in one of the two phases. The authors discuss several choices for their problem. The main result is that in the case of a small slope of the Clausius-Clapeyron curve as in our case, all requirements are equivalent to Eq. (A14).

Instead of the temperatures T_2,T_1 at the confining plates, the control parameters $\Delta T=T_1-T_2$ and z_0 have been used in our analysis. The material parameters for 5CB are taken from Ref. [8]. For a given z_0, the weighted average is always used (we will leave out the bar in the following). In line with Ref. [5], d, d^2/κ, and $(\nu\kappa)/(\alpha g d^3)$ are used as scales for length, time, and temperature, respectively. The surface tension σ for the nematic-isotropic interface is 1.4×10^{-5} J/m^2 [36], i.e., 5.5×10^{-2} in our units of $g\Delta\rho d^2$.

Adding up $\partial^2/\partial x\partial z$ applied to the x component (u) and $-\partial^2/\partial x^2$ applied to the z component (w) of $\mathbf{v}$ in Eq. (A2a), one ends up with

$$\frac{\kappa}{\nu}\nabla^2\frac{\partial\theta}{\partial t}=\nabla^4 f-\left[P\left(1+\sigma\frac{\partial^2}{\partial x^2}\right)\delta(z-z_0)+1\right]\theta, \tag{A15}$$

$$[1+R_\beta\delta(z-z_0)]\frac{\partial\theta}{\partial t}=\nabla^2\theta-[R_Q\delta(z-z_0)+R]\frac{\partial^2}{\partial x^2}f, \tag{A16}$$

with the velocity potential defined in (A7) and $\nabla^2=\partial^2/\partial x^2+\partial^2/\partial z^2$. The following dimensionless control parameters have been defined:

$$R=\frac{gd^3}{\nu\kappa}(\alpha\Delta T),\quad R_Q=\frac{gd^3}{\nu\kappa}(\alpha Q/C_p),$$

$$R_{\Delta\rho}=\frac{gd^3}{\nu\kappa}(\Delta\rho/\rho). \tag{A17}$$

Their relative magnitude is described by the ratios [37]

$$P=\frac{R_{\Delta\rho}}{R},\quad R_\beta=\frac{R_Q}{R}. \tag{A18}$$

The discontinuities of the z derivatives are made explicit in terms of the δ-functions at the interface z_0. By integrating with respect to z the (rescaled) jump conditions [Eqs. (A9) and (A10)] [with η inserted from Eq. (A14)] are easily recovered.

The physical interpretation of the parameters in Eq. (A17) is quite obvious, since they characterize the different destabilization mechanism. The parameter R is the familiar Rayleigh number describing thermal buoyancy. The other parameters are only active at the interface: In R_Q the latent-heat term Q/C_p replaces ΔT and in $R_{\Delta\rho}$ the gravitational acceleration $g\Delta\rho/\rho$ appears instead of the buoyant acceleration $g\alpha\Delta T$. Note that in Ref. [12] a slightly different scaling was adopted; temperature was measured in units of Q/C_p, which might be more convenient when considering the limit $\Delta T\rightarrow 0$.

The determination of the convection threshold is standard, though tedious [38]. The equations separate with respect to their vertical coordinate z, the ''infinitely'' extended horizontal coordinate x, and the time t; the dependence on the latter variables is captured by the factor $\exp(\gamma t+ipx)$. With respect to z the solutions can be written as a linear combination of exponentials $\exp(\pm\zeta_i z)$, separately for each of the domains $z>z_0$, $z<z_0$. The eigenvalues ζ_i, $i=1$, 2, and 3, which depend on p and the control parameters in Eq. (A15), are the roots of a cubic equation. It is easy to see that one arrives at a linear homogeneous system for 12 expansion coefficients, corresponding to six boundary conditions at $z=1$ and 0 and another six at the interface $z=z_0$. For nontrivial solutions of this system, the determinant has to vanish. One arrives at a complicated equation which connects for given wave number p the growth rate γ with R, z_0, and the other parameters in Eqs. (A17) and (A18). Stationary convection at onset corresponds to a vanishing growth rate γ, and yields the neutral curve $R_0(p)$ with its minimum at the critical wave number $p=\alpha_c$. After the determination of the stationary threshold we always checked whether an oscillatory onset might have preceded: we never found any, in line with Ref. [12]. The explicit (in detail quite tricky) manipulations have been done with the help of the well known MAPLE package, which allows for symbolic as well as numerical calculations. For instance, when dealing with the exponentials in the determinant, it was very convenient that the calculations with MAPLE can be done with arbitrary numerical accuracy.

[1] See, for instance, P. G. de Gennes and J. Prost, *The Physics of Liquid Crystals* (Clarendon Press, Oxford, 1993); S. Chandrasekhar, *Liquid Crystals* (Cambridge University Press, London, 1992); L. M. Blinov and V. G. Chigrinov, in *Electro-optic Effects in Liquid Crystal Materials* (Springer, New York, 1994).

[2] A. Buka and L. Kramer, in *Pattern Formation in Liquid Crystals* (Springer, New York, 1996).

[3] L. Kramer and W. Pesch, Annu. Rev. Fluid Mech. **27**, 515 (1995).

[4] S. Chandrasekhar, *Hydrodynamic and Hydromagnetic Stability* (Oxford University Press, London, 1961).

[5] F. H. Busse, in *The Fluid Mechanics of Astrophysics and Geophysics, Vol. 4, Mantle Convection, Plate Tectonics, and Global Dynamics*, edited by W. R. Peltier (Gordon and Breach, New York, 1989).

[6] M. C. Cross and P. C. Hohenberg, Rev. Mod. Phys. **65**, 851 (1993).

[7] For a recent review, see G. Ahlers, in *Pattern Formation in Liquid Crystals* (Ref. [2]).

[8] L.I. Berge, G. Ahlers, and D.S. Cannell, Phys. Rev. E **48**, R3236 (1994).

[9] E. Plaut and R. Ribotta, Europhys. Lett. **38**, 441 (1997); Phys. Rev. E **56**, R2375 (1997); Eur. Phys. J. B **5**, 265 (1998); **5**, 283 (1998).

[10] L. Thomas, W. Pesch, and G. Ahlers, Phys. Rev. E **58**, 5884 (1998).

[11] E. Plaut and W. Pesch, Phys. Rev. E (to be published).

[12] F. Busse and G. Schubert, J. Fluid Mech. **46**, 801 (1971).

[13] D. E. Fitzjarrald, J. Fluid Mech. **102**, 85 (1981).

[14] J. Salan and E. Guyon, J. Fluid Mech. **126**, 13 (1983).

[15] G. Ahlers, L. I. Berge, and D. S. Cannell, Phys. Rev. Lett. **70**, 2399 (1993).

[16] See, for instance, H. J. Kull, Phys. Rep. **206**, 197 (1991), and numerous references therein.

[17] G. Schubert and J. M. Straus, J. Geophys. Res. **85**, 6505 (1980); Nature (London) **287**, 423 (1980); [see the remark in *The Fluid Mechanics of Astrophysics and Geophysics)* (Ref. [5])].

[18] For an interesting brief description of the current status of understanding of the mantle-convection problem, see R. A. Kerr, Science **258**, 1576 (1992).

[19] In the literature on two-phase convection it is customary to define the latent heat to be *positive* when released in the transition from the lighter to the denser phase [see *The Fluid Mechanics of Astrophysics and Geophysics* (Ref. [5]) below Eq. 6.1].

[20] G. Ahlers, D. S. Cannell, L. I. Berge, and S. Sakurai, Phys. Rev. E **49**, 545 (1994).

[21] We obtained our 5CB from EM Industries, 5 Skyline Drive, Hawthorne, NY 10532.

[22] A. Schlüter, D. Lortz, and F. Busse, J. Fluid Mech. **23**, 129 (1965).

[23] See, for instance, F. Busse, J. Fluid Mech. **30**, 625 (1967).

[24] Q. Feng, W. Pesch, and L. Kramer, Phys. Rev. A **45**, 7242 (1992).

[25] See Appendix B of G. Ahlers, in *Pattern Formation in Liquid Crystals* (Ref. [7]) for a summary of the fluid properties of 5CB.

[26] For $\sigma=0$ we have for instance for $\Delta T_c=1\,^\circ$C an increase of α_c roughly by a factor of 1.5.

[27] E. Dubois-Violette, Solid State Commun. **14**, 767 (1974).

[28] G. Schubert and J.M. Strauss, J. Geophys. Res. **85**, 6505 (1980).

[29] V. S. Arpaci and P. S. Larsen, in *Convection Heat Transfer* (Springer, New York, 1984).

[30] D. E. Hsieh and S. P. Ho, *Wave and Stability in Fluids* (World Scientific, Singapore, 1994).

[31] D. D. Joseph and Y. Renardy, *Fundamentals of Two-Fluid Dynamics I* (Springer, New York, 1992).

[32] R. W. Zeren and W. C. Reynolds, J. Fluid Mech. **53**, 305 (1972) [see, in particular, Eqs. (21) and (22) of this reference].

[33] D. A. Nield, J. Fluid Mech. **19**, 341 (1964).

[34] J. R. A. Pearson, J. Fluid Mech. **4**, 489 (1958).

[35] A. Huang and D. D. Joseph, J. Fluid Mech. **242**, 235 (1992).

[36] S. Faetti and V. Palleschi, J. Chem. Phys. **81**, 6254 (1984).

[37] For geophysical applications additional contributions in R_β and in P have to be considered (see Ref. [12]).

[38] A. Tschammer, Ph.D. thesis, Universität Bayreuth, Bayreuth, Germany, 1996 (unpublished).